

The ultraviolet upturn in brightest cluster galaxies

S. I. Loubser¹* and P. Sánchez-Blázquez^{2,3,4}

¹Unit for Space Physics, North-West University, Potchefstroom 2520, South Africa

²Instituto de Astrofísica de Canarias, E-38200 La Laguna, Tenerife, Spain

³Departamento de Astrofísica, Universidad de La Laguna, E-38205 La Laguna, Tenerife, Spain

⁴Departamento de Física Teórica, Módulo C15, Universidad Autónoma de Madrid, E28049 Cantoblanco, Spain

Accepted 2010 September 3. Received 2010 July 27. in original form 2010 April 21

ABSTRACT

This paper is part of a series devoted to the investigation of a large sample of brightest cluster galaxies (BCGs), their properties and the relationships between these properties and the properties of the host clusters. In this paper, we compare the stellar population properties derived from high signal-to-noise ratio, optical long-slit spectra with the *Galaxy Evolution Explorer* (GALEX) ultraviolet (UV) colour measurements for 36 nearby BCGs to understand the diversity in the most rapidly evolving feature in old stellar systems, the UV upturn. We investigate (1) the possible differences between the UV upturn of BCGs and that of a control sample of ordinary ellipticals in the same mass range, as well as possible correlations between the UV upturn and other general properties of the galaxies; (2) the possible correlations between the UV upturn and the properties of the host clusters and (3) the recently proposed scenarios where helium sedimentation in the cluster centre can produce an enhanced UV upturn. We find systematic differences between the UV colours of BCGs and ordinary ellipticals, but we do not find correlations between these colours and the properties of the host clusters. Furthermore, the observations do not support the predictions made by the helium-sedimentation model as an enhancer of the UV upturn.

Key words: galaxies: elliptical and lenticular, cD – galaxies: evolution – galaxies: stellar content – ultraviolet: galaxies.

1 INTRODUCTION

The ultraviolet (UV) upturn, first discovered by Code & Welch (1979), is the rising flux with a decreasing wavelength from 2500 Å to the Lyman limit observed in the spectrum of some massive elliptical galaxies (see O’Connell 1999 for a review).

In spiral and irregular galaxies, flux emitted in the UV acts as an excellent measure of the current star formation rate (Gil de Paz et al. 2007). In the case of (mostly quiescent) early-type galaxies, the flux at wavelengths shorter than 1800 Å [far-UV (*FUV*)] is believed to be produced by hot, low-mass horizontal branch (HB) stars, although the mechanism with which an old population can develop hot stars is still hotly debated (see Yi 2008). For the non-quiescent, low-redshift elliptical galaxies, analysis of UV wavelengths longer than 1800 Å [near-UV (*NUV*)] is a useful indicator of residual star formation (Pipino et al. 2009). Possible solutions for the origin of the increase in *FUV* flux in quiescent early-type galaxies include metal-rich stars that lose mass and become HB stars, metal-poor stars that evolve to very high temperatures and on to the HB, or mass transfer in binary systems that can expose the hot core of an HB star (Donahue

et al. 2010). These theoretical scenarios make different predictions about the correlations between the strength of the UV upturn and the metallicity as well as about the evolution of this feature with redshift in passively evolving systems. Observations of the evolution of the *FUV* – *V* colours of brightest cluster galaxies (BCGs) with redshift seem to prefer the single stars hypothesis to the binary theory (Ree et al. 2007). However, the metal-poor and metal-rich hypotheses also have problems. For example, a large fraction of metal-poor stars are needed to explain the strength of the UV upturn observed in elliptical galaxies and the metal-rich scenario seems to require mass losses from red giant branch stars much larger than those predicted theoretically.

A popular third possibility, which seems to solve some of the problems associated with the HB hypotheses, is the enhanced helium abundance hypothesis. This hypothesis is motivated by globular cluster observations containing peculiar features in the colour–magnitude diagram that can only be explained by the presence of super-helium-rich sub-populations (D’Antona & Caloi 2004; Norris 2004; D’Antona et al. 2005; Lee et al. 2005; Piotto et al. 2005). These populations could be a major source of *FUV* flux in quiescent elliptical galaxies, although studies suggest that the deduced value of the helium abundance is too small to be influential on galactic scales (Lee et al. 2005; Yi 2008). However, in the centres of

*E-mail: Ilani.Loubser@nwu.ac.za

clusters, an extra source of helium could come from sedimentation processes (Peng & Nagai 2009). If the helium sedimentation mechanism is important, the UV upturn strength in the BCGs could be greatly enhanced. In fact, it is known from observations of nearby early-type galaxy samples that BCGs are most likely the strongest UV emitters among the quiescent early-type galaxies in each redshift bin (Burstein et al. 1988; Boselli et al. 2005; Donas et al. 2007).

If the mechanism producing the UV upturn in BCGs is different than that of ordinary elliptical galaxies, then the results on the evolution of the UV colours with redshift mentioned above will not necessarily be representative for the whole population of objects hosting old stellar populations. In fact, Atlee, Assef & Kochanek (2009) obtained very different results for UV-colour evolution using a sample of ordinary bright elliptical galaxies.

In this work, we want to explore the mechanism(s) producing the UV upturn in BCGs and compare it with that producing the UV upturn in elliptical galaxies by studying the relation between the UV-upturn strength and other properties of the galaxies. Several authors have found correlations between the strength of the UV upturn and the Mg index, an indicator of metallicity, in early-type galaxies (Burstein et al. 1988; Donas et al. 2007; but also see Rich et al. 2005). The question remains whether correlations between the UV upturn and the spectral properties of BCGs exist, which will provide us with further clues to the origin of the UV upturn.

This paper is the third in a series of papers investigating an overall sample of 49 BCGs in the nearby Universe for which we have obtained high signal-to-noise ratio, long-slit spectra on the Gemini telescopes and William Herschel Telescope (WHT). This large, spatially resolved, spectroscopic sample of BCGs allows possible connections between the kinematical, dynamical and stellar population properties to be studied. The first paper was devoted to the spatially resolved kinematics of the BCGs (Loubser et al. 2008, hereafter Paper I). In the second paper, we derived single stellar population (SSP)-equivalent ages, metallicities and α -abundance ratios in the centres of the galaxies and then systematically compared these with a sample of ordinary elliptical galaxies as well as with the host cluster properties (Loubser et al. 2009, hereafter Paper II).

Here, we turn our attention to the UV upturn and its correlations with the properties derived from the optical spectra as well as with the host cluster environment. Our BCG sample has the advantage of having detailed X-ray values of the host cluster properties available from the literature, which BCGs extracted from the Sloan Digital Sky Survey (SDSS) lack. The spectra in this BCG sample also have significantly improved signal-to-noise ratios compared to previous samples (Crawford et al. 1999, and references therein). Most of the previous observational studies of BCGs in the UV concentrate on detecting star formation using the *NUV* measurements, and in mainly cooling flow clusters (Pipino et al. 2009; Donahue et al. 2010; Hicks, Mushotzky & Donahue 2010; Wang et al. 2010, but also see O’Dea et al. 2010 for *FUV* measurements). Here, we investigate the variations in the UV upturn, which in turn can cause scatter in the star formation relations derived. In Section 2, we describe the UV and optical data. In Section 3, we compare the UV upturn measured for the BCGs to that measured for a control sample of ordinary ellipticals matched in mass range and distribution. In Section 4, we test the model predictions by Peng & Nagai (2009), who predict that the UV-upturn phenomenon should be most pronounced in BCGs hosted by high-mass, dynamically relaxed and cool-core clusters. In Section 5, we investigate possible correlations between the UV upturn and the luminosity-weighted age and metal-

licity for the BCGs and ordinary elliptical samples. We summarize our findings in Section 6.

2 DATA

We briefly review the relevant selection criteria and properties of the resulting sample (detailed in Paper I) here. The sample consists of the dominant galaxies closest to the X-ray peaks in the centres of their host clusters. We adopt the definition to comply with recent literature (e.g. De Lucia & Blaizot 2007; Von der Linden et al. 2007), where the central, dominant galaxy in a cluster is referred to as the BCG. According to the above definition, for a small fraction of clusters the BCG might not strictly be the brightest galaxy in the cluster.

We initially intended to investigate a subsample of BCGs with extended haloes (cD galaxies). However, due to the difficulties in the classification of cD galaxies and the very inhomogeneous definitions in the literature, we cannot be confident that all the galaxies in our sample are cD galaxies. Instead, we can say that our sample comprises the dominant galaxies closest to the X-ray peaks in the centres of clusters. The sample selection combined three methods making the best use of available information from the literature and astronomical data bases: the two well-known galaxy cluster classification systems that distinguish clusters containing a cD galaxy in the centre from other galaxy clusters (Bautz & Morgan 1970; Rood & Sastry 1971), an all-sky search in the HyperLEDA¹ data base for galaxies with T-types between -3.7 and -4.3 (the de Vaucouleurs Third Reference Catalogue classifies cD galaxies as T-type = -4) and galaxies that break the de Vaucouleurs $r^{\frac{1}{4}}$ law at large radii.

In summary, the 49 BCGs in our overall sample were either classified as cD in NASA/IPAC Extragalactic Database (NED) or had profiles breaking the $r^{\frac{1}{4}}$ law in the external parts. The following global criteria were applied to the sample: apparent *B* magnitude brighter than 16, distance closer than 340 Mpc and an absolute magnitude cut-off at $M_B = -20$. The sample is not complete over any of these parameters, and no UV or X-ray criteria were involved in the selection. Nevertheless, the galaxies are hosted by clusters with a wide range of X-ray luminosities from $L_X = 0.03 \times 10^{44}$ to $17.07 \times 10^{44} \text{ erg s}^{-1}$, and it includes BCGs hosted by cooling flow and non-cooling flow clusters.

For this optically selected sample, high signal-to-noise ratio, long-slit spectra were obtained at the Gemini and WHT telescopes. The spectroscopic data, together with the reduction procedures, were presented in Papers I and II, and are not repeated here. The overall BCG sample has 36 galaxies with *FUV* and *NUV* measurements in the *Galaxy Evolution Explorer* (*GALEX*) data base (ranging from $FUV - NUV = 0.20$ to 1.32), which will be analysed further. This subsample of BCGs (still hosted by clusters with a wide range of X-ray luminosities from $L_X = 0.04 \times 10^{44}$ to $17.07 \times 10^{44} \text{ erg s}^{-1}$) is representative of our overall BCG sample. Information from *ROSAT* X-ray data on the properties of the host clusters was collected from the literature (see Section 4). Of these 36 BCGs, 18 have X-ray temperature (T_X) measurements, 27 cluster velocity dispersion (σ_{cluster}) measurements and 30 X-ray offset (R_{off}) measurements. All the galaxy and host cluster properties used here are listed in Table A1.

The *GALEX FUV* (1344–1786 Å) and *NUV* (1771–2831 Å) magnitudes and their errors were extracted from the *GALEX* data base²

¹ <http://leda.univ-lyon1.fr/>

² <http://galex.stsci.edu/GR4/>

(see Martin et al. 2005). Positional cross-correlation of the UV sources in the data base was performed within 6 arcsec of the optical source coordinates, and the UV images were examined by eye to ensure that none of the sources was mismatched and that the sources were not near the edge of the detector. In each case, the *NUV* and *FUV* magnitudes and errors were taken from the longest exposures in the *GALEX* data base and were mainly from the All-sky Imaging Survey. The extracted *NUV* and *FUV* magnitudes were taken from *SEXTRACTOR* ‘mag_auto’ and were the total magnitudes within an elliptical aperture that was scaled to 2.5 times the Kron diameter as determined from the *NUV* and *FUV* images, respectively (Kron 1980; Bertin & Arnouts 1996). To minimize aperture effects and instrumental inhomogeneities, we chose to characterize the UV upturn as the *FUV* – *NUV* colour, based on *GALEX* measurements alone. In addition, there is a lack of enough homogeneous *V* (or *r*) magnitudes available in the literature to keep our sample statistically significant if we characterize the UV upturn as *FUV* – *V*. We recalculated the *FUV* magnitudes so that the effective *FUV* apertures were equal to the *NUV* apertures, by using the flux measurements from the *GALEX* data base and the AB magnitude system of Oke & Gunn (1983). The *GALEX* data base defines the *NUV* and *FUV* magnitudes as $m_{UV} = m_0 - 2.5 \log f_{UV}$, where f_{UV} is the count rate and $m_0 = 20.082$ (*NUV*) and 18.817 (*FUV*) (Morrissey et al. 2005). The uncertainty in these zero-points is ± 0.15 mag for both *FUV* and *NUV* (Donas et al. 2007). We propagate the errors on the magnitudes, extracted from *GALEX*, throughout the study.

Internal extinction is small in most nearby early-type galaxies, and the *FUV* – *NUV* colour is essentially reddening free for moderate amounts of reddening. We expect a very low impact of the internal extinction on the scatter of the measurements, and as these corrections are very uncertain, we do not include them.

To quantify the effect of Galactic reddening, the Galactic extinction was inferred from the 100- μ m dust emission maps of Schlegel, Finkbeiner & Davis (1998). Using the extinction law of Cardelli, Clayton & Mathis (1989), Wyder et al. (2007) calculated $\frac{A_{FUV}}{E(B-V)} = 8.24$ and $\frac{A_{NUV}}{E(B-V)} = 8.20$, which gives corrections in the *FUV* – *NUV* colours of $\ll 0.01$ mag, for the $E(B-V)$ values derived for the galaxies in our sample.³ Hence, these corrections are negligible and not included here. Similarly, at the low redshift of this sample (mean $z = 0.0374 \pm 0.0029$), the *K*-corrections to the magnitudes are negligible.

One of the goals of this study is to compare the behaviour of the UV upturn in BCGs with a control sample of ordinary elliptical galaxies. Stellar populations in early-type galaxies seem to be strongly correlated with the central velocity dispersion, and thus we choose to compare the UV upturn of the BCG sample with a control sample of normal elliptical galaxies with the same range of central velocity dispersion (which we use as a proxy for mass). For this control sample of normal elliptical galaxies, we use the sample of Sánchez-Bláquez et al. (2006, hereafter SB06) in the same mass range as the sample of BCGs, and excluding any known BCGs. The complete SB06 sample consists of 98 galaxies, of which 35 belong to the Coma cluster and the rest are galaxies in the field, in groups or in the Virgo cluster. The SB06 control sample has 37 galaxies with *FUV* and *NUV* measurements in the *GALEX* data base. We performed a Kolmogorov–Smirnov (K–S) test on the velocity dispersion distributions of the two subsamples for which UV measurements were available within the $\log \sigma = 2.25$ – 2.65 km s^{−1}

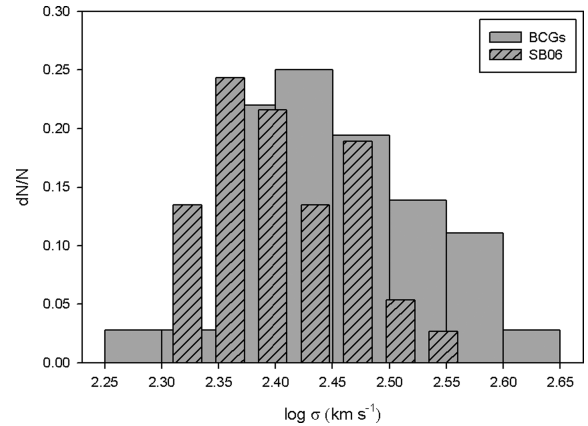


Figure 1. The velocity dispersion distributions of the SB06 (grey – striped) and the BCG (grey – solid) subsamples with UV measurements.

range (shown in Fig. 1), where the null hypothesis is that the distributions were drawn from an identical parent population. The two velocity dispersion distributions are consistent and have a test value of 0.260, where a test value larger than $D = 0.290$ indicates that the two samples compared are significantly different from each other at the 95 per cent confidence level. We used the same procedure described above to extract *FUV* – *NUV* colours for the control sample.

Five galaxies in our BCG sample have *GALEX* *NUV* and *FUV* measurements which were used in previous studies with similar apertures (Donas et al. 2007; Ree et al. 2007). In these studies, the magnitudes were extracted directly from the images by the authors. We detect no systematic difference between our *FUV* – *NUV* measurements and errors and those of the previous studies plotted in Fig. 2. There is one galaxy (UGC 00579) in the Donas et al. (2007) sample with a very different colour value. We have investigated this galaxy and found no reason for this difference, and we have checked that including it in the sample makes no difference to any of the plots and conclusions. For the rest of the galaxies, the values presented here and those measured in the other studies agree within the errors.

The weak optical emission lines present in some of the BCG spectra most likely indicate active star formation regions or active

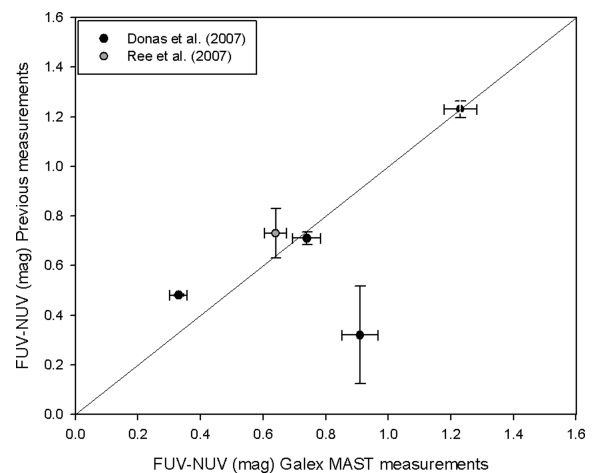


Figure 2. Comparison between the measurements extracted from the *GALEX* archive against previous measurements by different authors directly from the images.

³ When different values such as $\frac{A_{FUV}}{E(B-V)} = 8.24$ and $\frac{A_{NUV}}{E(B-V)} = 8.10$ (Atlee et al. 2009) are used, the corrections remain negligible.

galactic nuclei (AGN; Edwards et al. 2007; Von der Linden et al. 2007), both of which can alter the UV properties of the galaxies. For example, there has been some suggestion that a relatively small number of young stars can contribute to the observed scatter in the UV upturn (Donas et al. 2007; Han, Podsiadlowski & Lynas-Gray 2007). To isolate those galaxies whose UV spectra may be contaminated by star formation or AGN, we identify the BCGs containing emission lines in their optical spectra, using the GANDALF routine⁴ (Sarzi et al. 2006) as described in Paper II. The galaxies with detected emission lines will be indicated separately in some of the figures. Of the 36 BCGs studied here, eight have been identified as containing emission lines in their spectra (see Paper II).

We measured the individual emission lines and plotted them on a [O III] λ 5007/H β against [O II] λ 3727/H β diagram (as [N II] λ 6584 and H α were outside our wavelength range) to separate the two major origins of emission: star formation and AGN (Baldwin, Phillips & Terlevich 1981; Lamareille et al. 2004) in Paper II. We found all nine galaxies for which the H β , [O II] λ 3727 and [O III] λ 5007 lines could be measured (within at least 2σ detections) to be star-forming galaxies according to this test. Because the diagnostic diagram used in Paper II is much less effective at separating different sources of ionization (Stasińska et al. 2006), and because the fraction of the current sample containing emission lines is relatively small, and with weak emission lines, we do not draw detailed conclusions about the nature of emission lines in BCGs here. It can be seen from Figs 3, 4, 6 and 7 that including or excluding the emission-line BCGs in this study does not influence the conclusions drawn from these plots. It can also be seen in Fig. 3 that these galaxies are not necessarily bluer in $FUV - NUV$ than the quiescent galaxies.

Several previous studies which observed BCGs in the NUV (which is sensitive to the detection of young stars) have found a relation between BCGs which show evidence of recent star formation episodes and cooling flows in their host clusters (Mittaz et al. 2001; Martel et al. 2002; O’Dea et al. 2004; Hicks & Mushotzky 2005; Rafferty, McNamara & Nulsen 2008; Pipino et al. 2009; Hicks, Mushotzky & Donahue 2010). However, not all BCGs in cooling flows show significant star formation (Quillen et al. 2008). The UV upturn is observed in the FUV (which is more sensitive to the HB stars), but as mentioned above, it is important to assess the influence of possible small episodes of recent star formation, as detected in the NUV , on our measurements. Rafferty et al. (2008) found that active star formation in BCGs depends on the presence of cooling flow clusters with short cooling times, with the additional requirement of the BCG being located close to the X-ray centre (~ 20 kpc). It is therefore also of interest to identify the BCGs hosted by cooling flow clusters, to assess the effects of possible cooling-flow-induced star formation in the sample.

We use different symbols in some of the plots to indicate galaxies hosted by cooling flow clusters, host clusters with definite non-detections of cooling flows and host clusters for which no cooling flow information could be found. Several definitions for cooling flow clusters exist in the literature, often based on central temperature drop, short cooling time or significant mass deposition rates. We extract the cooling flow information (see Table A1), based on mass deposition rates, mainly from White, Jones & Forman (1997) and substitute it with information from Rafferty et al. (2006), Edwards et al. (2007) and Giovannini, Liuzzo & Giroletti (2008). The information on the galaxies in common between these studies agree very

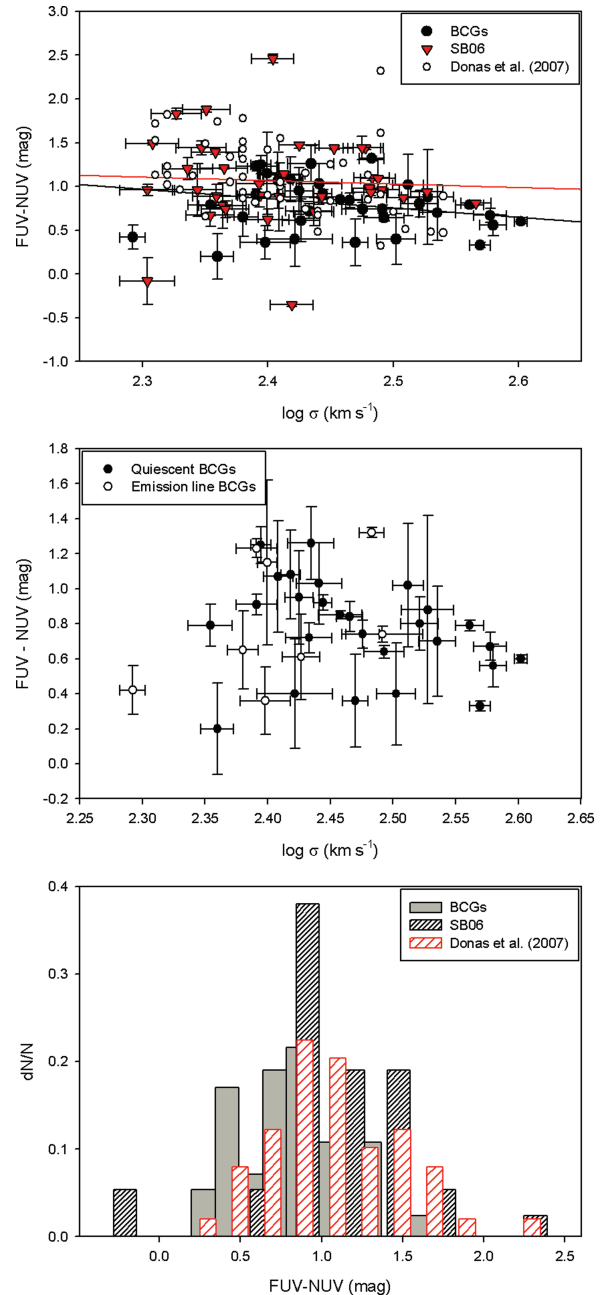


Figure 3. The top panel shows the $FUV - NUV$ colour against velocity dispersion for BCGs and non-BCGs. The middle panel shows the $FUV - NUV$ colour against velocity dispersion for just the BCGs, where the filled symbols indicate the quiescent BCGs and the empty symbols indicate the emission-line BCGs. The bottom panel shows the histogram of the $FUV - NUV$ colour distributions of the BCGs and non-BCGs.

well. Of the eight emission-line galaxies, two are hosted by cooling flow clusters, three by non-cooling flow clusters and three clusters’ cooling flow status is not known. Of the 28 quiescent BCGs, eight are in cooling flow clusters, 11 in non-cooling flow clusters and nine not known.

The assessment of the impact of star formation on the UV colours is difficult to do, because the main contributors to these colours are still a matter of debate. Stellar population models including post-asymptotic giant branch stars (but not extreme HB stars) indicate that $FUV - NUV$ colours are indeed sensitive to the age of the

⁴ We make use of the corresponding PPF and GANDALF IDL (Interactive Data Language) codes which can be retrieved at <http://www.leidenuniv.nl/sauron/>.

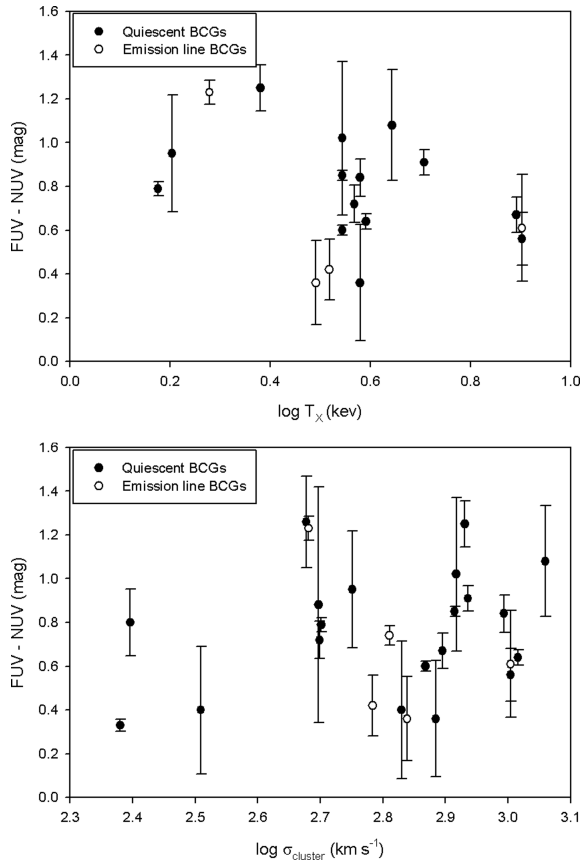


Figure 4. $FUV - NUV$ colour against the X-ray temperature and velocity dispersion of the host clusters.

population, but not more than $FUV - V$ colours, for example. In a population composed of old stars with a small fraction of young stars, the $FUV - NUV$ colours are affected only when the age of the burst is between 1 and 2 Gyr (the exact limits depend on the fraction of young stars; see fig. 12 in Rampazzo et al. 2007). To conclude, we have tested that even if we take only galaxies in non-cooling flow clusters and without emission lines, our conclusions hold.

3 THE UV UPTURN AS A FUNCTION OF MASS IN BCGS VERSUS NON-BCGS

Donahue et al. (2010) suggested that their sample of BCGs show less dispersion in their NUV -optical colours than that of ellipticals as a whole. They posed the question whether this uniformity in NUV meant that BCGs are less contaminated from star formation or are more uniform in their age and metallicity than their lower mass normal elliptical counterparts. To answer this question, and since stellar populations in early-type galaxies seem to be strongly correlated with the central velocity dispersion, as mentioned, we investigate the UV upturn ($FUV - NUV$ colour) of the BCG sample relative to the SB06 control sample of ordinary ellipticals in the same mass range.

We plot the $FUV - NUV$ colours for both the BCG and the control samples in the top panel of Fig. 3 and the histograms of the distributions in the bottom panel of Fig. 3. Straight line fits to the velocity dispersion plots were made for both samples with a least-squares fitting routine, and are also shown in the top panel of Fig. 3. Statistical t -tests were run to explore the presence of correlations. Even though neither of the two samples form a statistically

significant correlation with velocity dispersion (mass) at a 95 per cent confidence level, the BCG sample is much less scattered with velocity dispersion than the non-BCGs over the same mass range. The standard deviation on the mean colour values of the BCGs is 0.33 compared to 0.49 for the SB06 sample.⁵ The middle panel shows the $FUV - NUV$ colour against velocity dispersion for just the BCGs, where the filled symbols indicate the quiescent BCGs and the empty symbols indicate the emission-line BCGs. The outliers in this plot are discussed in Section 5. We do not find a clear distinction between the active and quiescent BCGs, which is in agreement with the findings of Burstein et al. (1988) for normal elliptical galaxies.

To eliminate the possibility that the absence of correlations is due to the small range in velocity dispersions (masses), we used the $FUV - NUV$ measurements of ellipticals presented by Donas et al. (2007). They found a clear correlation over a larger velocity dispersion range and used the same apertures as used here. We selected all the ellipticals in their sample (which includes some ellipticals in the centres of clusters) in the same velocity dispersion range used here ($\log \sigma = 2.30 - 2.65 \text{ km s}^{-1}$) and fitted a correlation and t -test as above. In this limited velocity dispersion range, we still find a correlation between the $FUV - NUV$ colour and velocity dispersion for their sample.

The histogram in Fig. 3 indicates another difference in the distributions of the $FUV - NUV$ colours of the BCG and non-BCG samples, with the ordinary ellipticals having larger $FUV - NUV$ colours (i.e. having a smaller UV upturn). We performed a K-S test on the $FUV - NUV$ colour measurement distributions of the two samples, where the null hypothesis is that the distributions were drawn from an identical parent population. We find that the distributions of the two samples compared are significantly different from each other at the 95 per cent confidence level (this has also been confirmed with a χ^2 test). The mean $FUV - NUV$ for BCGs is 0.791 ± 0.055 , whereas it is 1.062 ± 0.080 for the ellipticals.

To further test the validity of these findings, we also compare the UV colours of the BCGs with the UV colours of the Donas et al. (2007) ellipticals in the same apertures. We also plot the 49 ellipticals with $\log \sigma > 2.30 \text{ km s}^{-1}$ from the Donas et al. (2007) sample in the top and bottom panels of Fig. 3. The UV colours of the Donas et al. (2007) ellipticals in the same mass range are also more scattered compared to the BCGs (with a standard deviation on the mean colour values of 0.42 compared to 0.33 for the BCGs). We again find that the ellipticals have bigger $FUV - NUV$ colours than the BCGs (we find a mean $FUV - NUV$ colour of 1.089 ± 0.059 , compared to 0.791 ± 0.055 for the BCGs and to 1.062 ± 0.080 for the SB06 ellipticals). We find that the UV colour distributions of the two elliptical samples agree very well, whereas the distribution of the BCG sample is significantly different from both elliptical samples.

It is known that BCGs have larger sizes and lower optical surface brightness than non-BCGs of the same mass (Von der Linden et al. 2007). Since we are measuring the UV fluxes in a radius scaled to the Kron radius (which itself is roughly equal to the half-light radius), it could be that we are measuring a slightly bigger FUV and NUV aperture for the BCGs than for the non-BCGs, which could influence the $NUV - FUV$ colour measurements. Wang et al. (2010) simulated the differences arising in the $NUV - r$ measurements of BCGs purely because of their structural differences. They found

⁵ This is the intrinsic scatter since the standard deviations expected from the mean errors on the colour values are negligible.

the difference in the $NUV - r$ measurements (between the inner, R_{50} , and outer, R_{90} , galaxy apertures) to be 0.1 mag bigger for the BCGs than for the non-BCGs, purely as a result of their structure. The corresponding difference in the $FUV - NUV$ measurements can contribute to our result that the BCGs have a higher UV upturn than the non-BCGs, but it cannot fully explain the large differences in the distributions.

Wang et al. (2010) reported no difference between the $FUV - NUV$ colours of BCGs and those of non-BCGs from SDSS data; however, they cautioned that this might be ascribed to the lower quality of the FUV images used. It is to be noted that optically selected BCG samples have shown slightly different properties from X-ray-selected samples (see Burke, Collins & Mann 2000; Wang et al. 2010), and the properties derived from the two different samples can usually be reconciled if luminosity-dependent evolution is taken into account. However, this does not explain why our result differs from Wang et al. (2010), as their $FUV - NUV$ colour comparison was also based on an optically selected sample, and both samples define BCGs as the brightest galaxy closest to the centre of the cluster potential. Wang et al. (2010) also found this null result for both their inner, R_{50} , and outer, R_{90} , galaxy apertures; thus, the difference cannot be a result of different apertures.

We have also investigated how the scatter and range of the $FUV - NUV$ colours in our sample compare to samples of BCGs with definite recent star formation. Most of the previous samples, such as the cooling-flow-hosted BCGs which showed evidence of recent star formation in Pipino et al. (2009), are at intermediate redshifts ($z \sim 0.2-0.5$) and should not be directly compared. We identify the nearby BCGs ($z < 0.1$) with blue cores in the optical data presented by Rafferty et al. (2008) and find five of these BCGs with reliable $FUV - NUV$ measurements (calculated for the same apertures as used here). The $FUV - NUV$ colours of these five galaxies range from -1.01 to 0.51 mag (average of 0.06 , with a standard deviation of 0.62). If we compare this value with the average (and standard deviation) found for the $FUV - NUV$ colours of cooling-flow-hosted BCGs in our sample (0.68 ± 0.28), and for non-cooling-flow-hosted BCGs (0.80 ± 0.31), then we do not seem to see a strong influence of possible star formation connected to cooling flow clusters in our $FUV - NUV$ measurements. Hence, the relative homogeneity of the $FUV - NUV$ colours in the sample here might be used as evidence against recent episodes of star formation, since the range and scatter of $FUV - NUV$ colours expected for such episodes are large compared to the scatter in our BCG sample. We do not analyse this further as our main focus is the variations in the UV upturn (caused by HB stars).

4 ORIGIN OF THE UV UPTURN: TESTING MODEL PREDICTIONS

Stars with high helium abundance can become UV bright more easily, and therefore it is believed that helium abundance can make the UV upturn more pronounced (Dorman, O'Connell & Rood 1995; Yi, Demarque & Oemler 1997).

It has been suggested that helium sedimentation occurs in the intracluster medium (ICM) of galaxy clusters (Abramopoulos, Chanan & Ku 1981; Gilfanov & Syunyaev 1984; Qin & Wu 2000; Chuzhoy & Nusser 2003; Ettori & Fabian 2006; Peng & Nagai 2009). Under the influence of gravity, the heavier helium nuclei accumulate at the centres of massive galaxy clusters and can produce significant amounts of He abundance ($\Delta Y > 0.25$) in the central regions of hot, massive clusters. If the UV upturn is produced by extreme HB stars, the helium sedimentation process may help to

make it more pronounced in those galaxies in the centres of the clusters. The UV-upturn phenomena should be most pronounced in high-mass (or X-ray temperature), low-redshift and dynamically relaxed systems according to the Peng & Nagai (2009) model. The effect of helium sedimentation, and thus UV upturn, should also be larger for BCGs in cool-core clusters than in non-cool-core clusters.

In particular, the Peng & Nagai (2009) model predicts the following.

(i) *The UV upturn correlates with X-ray temperature (T_X) and the velocity dispersion of the host clusters (σ_{cluster}).* We use T_X and σ_{cluster} as proxies for the mass of the host cluster and use the values from Table A1 to plot Fig. 4. All the values are from spectra observed in the $0.1-2.4$ keV band with *ROSAT*, and using the same cosmology, namely the Einstein-de Sitter model of $H_0 = 50 \text{ km s}^{-1} \text{ Mpc}^{-1}$, $\Omega_m = 1$ and $\Omega_\Lambda = 0$. We do not convert to the concordance model, as the X-ray temperature and cluster velocity dispersion are independent of the cosmological model assumed (White et al. 1997; Bohringer et al. 2004). All the values for X-ray temperature (T_X in keV) are from White et al. (1997). We find no clear evidence that the $FUV - NUV$ colours correlate with T_X or σ_{cluster} in Fig. 4.

(ii) *The UV upturn is more pronounced in BCGs than in non-BCGs, and in BCGs hosted by cooling flow clusters than hosted by non-cooling flow clusters.* The former is plotted in Fig. 3 and the latter is plotted in Fig. 5. Fig. 3 showed significant differences in the distributions of the $FUV - NUV$ colours of the BCG and non-BCG samples, with the non-BCGs having more pronounced differences in $FUV - NUV$ (i.e. a lower UV upturn and much more scatter, as discussed in Section 3). We find no difference between the $FUV - NUV$ colours of the BCGs in cooling versus non-cooling flow clusters in Fig. 5.

It is interesting to note that Wang et al. (2010) found that among 21 X-ray-selected BCGs (12 in cooling flows), those located in clusters with central cooling times of less than 1 Gyr are significantly bluer than those located in clusters where the central gas cooling times are long. However, this was based on NUV measurements. Unfortunately, in most cases we lack the necessary X-ray information to determine the cooling time.

(iii) *The UV upturn correlates with the dynamical state of the clusters.* This is predicted as major mergers, for example, can destroy helium-rich cluster cores, producing some scatter in the UV upturn among BCGs. Numerical simulations predict that the offset

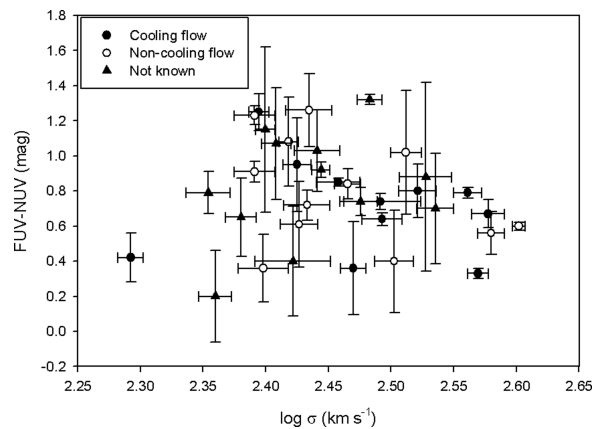


Figure 5. $FUV - NUV$ colour against the velocity dispersion for BCGs in cooling flows and non-cooling flows. Clusters with no cooling flow information available in the literature are also indicated.

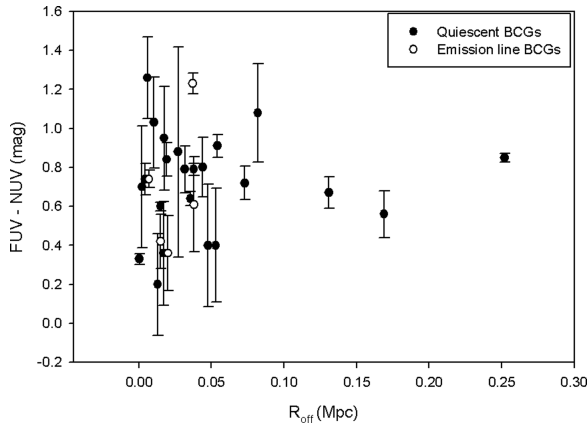


Figure 6. $FUV - NUV$ colour against the X-ray offset.

of the BCG from the peak of the cluster X-ray emission is an indication of how close the cluster is to the dynamical equilibrium state, and that this decreases as the cluster evolves (Katayama et al. 2003). Thus, the $FUV - NUV$ colours were plotted against the offset between the X-ray peak of the cluster and the BCG (R_{off}) in Fig. 6, where R_{off} is in Mpc and is from Table A1. We find no evidence of a correlation between the X-ray offset and $FUV - NUV$ colour.

The host clusters of our BCG sample cover a wide range in the parameters chosen to characterize them. The masses of the host clusters range from $\log \sigma_{\text{cluster}} = 2.3$ to 3.1 km s^{-1} , which includes groups to massive clusters. Similarly, the range of T_X and R_{off} is sufficient to detect possible trends (see Bildfell et al. 2008; Rafferty et al. 2008; Wang et al. 2010). In all cases, the errors on all the X-ray measurements are negligible compared to the scatter.

We also plotted Figs 4 and 6 distinguishing between cooling flow clusters, non-cooling flow clusters and clusters for which the information is not known, and we find no correlations.

In summary, we do find differences between the $FUV - NUV$ colour distributions of normal ellipticals and BCGs in the same mass range, as predicted by the models. We do not find strong further evidence in our data to support the predictions made from the models of Peng & Nagai (2009) that the UV-upturn phenomena should be most pronounced in BCGs hosted by high-mass, dynamically relaxed, cooling flow systems as a result of helium sedimentation. We also showed in Paper II that the BCG sample is not more uniform in age or metallicity than the SB06 sample in the same mass range. As such it is still an open question why we see differences, such as less scatter, between the $FUV - NUV$ colours of the BCGs compared to the normal ellipticals.

It is also interesting to note that Donahue et al. (2010) found no correlation between the NUV colour and optical luminosity, X-ray temperature, redshift or offset between the X-ray centroid and X-ray peak.

As mentioned in Section 2, we choose to characterize the UV upturn as the $FUV - NUV$ colour based on the *GALEX* measurements alone to minimize extinction and aperture effects and instrumental inhomogeneities. We note that this colour is not optimal for separating the effects of massive star formation from those of hot low-mass stars. To test whether this choice influences our results, we correlated the $FUV - NUV$ colours with $FUV - V$ colours for five BCGs in our sample which have homogeneous optical measurements in Sandage & Visvanathan (1978). We find a strong correlation between $FUV - NUV$ and $FUV - V$ within the errors [also see the correlation in fig. 7 of Ree et al. (2007) for their nearby galax-

ies]. We find that the scatter introduced in the $FUV - V$ values by the large, uncertain aperture corrections is larger than the intrinsic scatter in $FUV - NUV$.

5 OTHER CORRELATIONS

A correlation between the UV upturn and a property measurable from integrated light would not only help us to understand the origin of the UV upturn but can also be used to utilize the UV upturn as an age indicator (as discussed in Section 1).

For normal elliptical galaxies, the UV upturn is reported to correlate with Mg as well as with luminosity (Burstein et al. 1988; Donas et al. 2007; Gil de Paz et al. 2007). In particular, Gil de Paz et al. (2007) found elliptical galaxies with brighter K -band luminosities (i.e. more massive) to be redder in $NUV - K$ but bluer in $FUV - NUV$ than less massive ellipticals.

We plot the $FUV - NUV$ colour against the Two-Micron All-Sky Survey (2MASS) K magnitudes in Fig. 7, where we use different symbols to indicate emission-line BCGs and quiescent BCGs, and BCGs hosted by cooling flow and non-cooling clusters, respectively. We also plot the 2MASS K magnitudes of the SB06 sample of normal ellipticals in the top panel of Fig. 7. The K band is sensitive to the predominantly red populations in massive early-type galaxies and hence is a good measure of the total stellar mass. We do not correct the K magnitudes for passive evolution. Using the Bruzual & Charlot (2003) stellar population synthesis code with the assumption that the galaxies are 10-Gyr old and form in an instantaneous

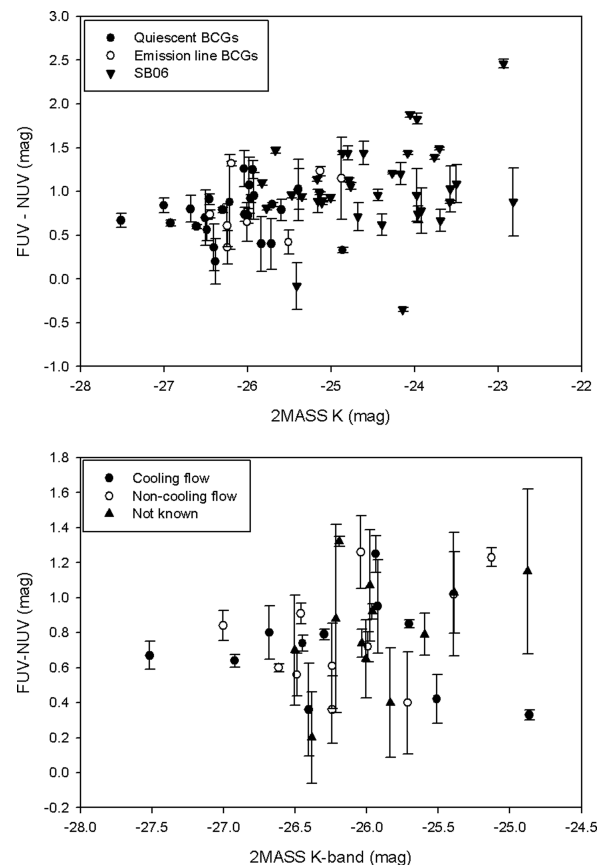


Figure 7. $FUV - NUV$ colour against the K -band luminosity. The top panel shows the SB06 sample of normal ellipticals for comparison. Clusters with no cooling flow information available in the literature are indicated in the bottom panel.

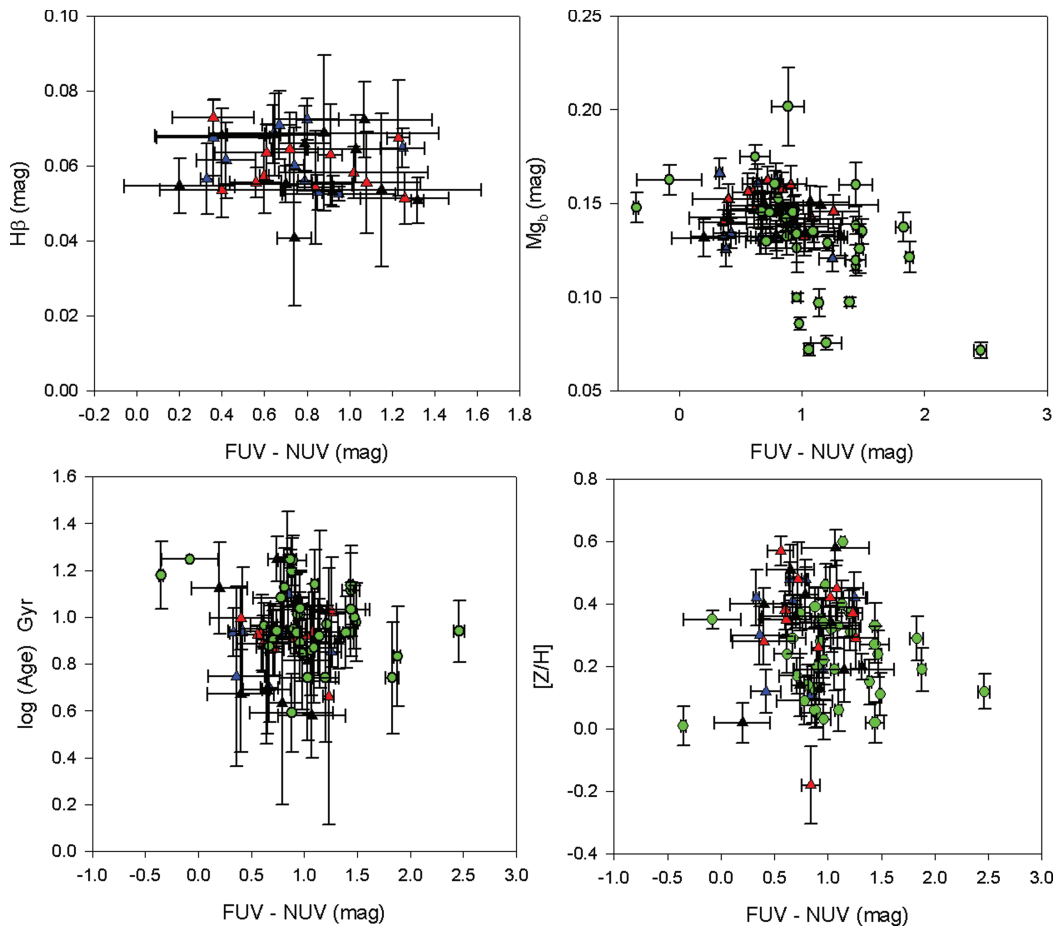


Figure 8. $FUV - NUV$ colour against $H\beta$ and $Mg\ b$ index measurements, age and metallicity. The green symbols are for the SB06 elliptical sample in the same mass range. The blue triangles are BCGs hosted by cooling flow clusters, the red are BCGs hosted by non-cooling flow clusters and the black are BCGs hosted by clusters whose cooling flow status is not known from the literature.

burst, this correction is only -0.2 mag for a galaxy at $z \sim 0.054$ (in the K band). Thus, it will not make a significant difference to whether or not a correlation is found.

We find no correlation with luminosity; however, it is interesting to note that when the galaxies with very low $FUV - NUV$ colour measurements are excluded ($FUV - NUV \lesssim 0.45$ mag), then correlations are found between the $FUV - NUV$ colour and luminosity⁶ as well as the $FUV - NUV$ colour and mass (Figs 3 and 5). The low $FUV - NUV$ colour measurements are not specific to lower/higher mass galaxies, galaxies with/without emission lines or galaxies hosted by cooling/non-cooling flow clusters. It is also not due to obvious systematic problems in the NUV and FUV measurements such as low exposure times for those galaxies. This is also the case for the outliers at the high end of $FUV - NUV$.

To analyse possible correlations between key absorption-line indices, such as $Mg\ b$, and the $FUV - NUV$ colours, we use the indices measured in the central apertures ($a_e/8$).⁷ We carefully calibrate these measurements to the widely used Lick/IDS system of absorption-line indices (detailed in Paper II) and plot the $H\beta$ and

$Mg\ b$ indices against the $FUV - NUV$ colour in Fig. 8. We use $Mg\ b$ instead of Mg_2 here, since it is less affected by systematic errors, for example flux calibration, and we remeasure the SB06 indices using the same procedure and plot them as reference. As the UV-upturn- $Mg\ b$ correlation is often interpreted as a metallicity effect on the UV flux, we also plot the $FUV - NUV$ colours against the luminosity-weighted age and metallicity ($[Z/H]$), derived using the predictions of Thomas, Maraston & Bender (2003) and Thomas, Maraston & Korn (2004). To avoid artificial offsets between samples due to the use of different techniques to calculate the SSP parameters, we recalculated these parameters for the sample of elliptical galaxies using exactly the same indices and method as used for our sample of BCGs. We find no significant correlation between $H\beta$ or $Mg\ b$ and $FUV - NUV$ colour (using a t -test), and as in Fig. 3, we find that the scatter in the $FUV - NUV$ colour measurements for BCGs is much less in the plots in Fig. 8 than for the ordinary ellipticals. As predicted by Yi & Yoon (2004), we do not find a correlation between α -enhancement ($[E/Fe]$) and $FUV - NUV$ colour (not shown here). In Paper II, we found that BCGs are more metal-rich and have higher α -abundance than the control sample of ellipticals, and here we have found that the BCGs have a higher UV upturn; however, the UV upturn does not clearly correlate with $[Z/H]$ or $[E/Fe]$. As mentioned in Section 2, excluding emission-line BCGs from these plots does not affect these conclusions.

Donas et al. (2007) found a tight anticorrelation between $FUV - NUV$ and the Mg_2 index for nearby early-type galaxies, and Boselli

⁶ This is clear in the bottom panel of Fig. 7, whereas the top panel shows that the BCG outliers are still within the scatter of the normal elliptical galaxies.

⁷ The effective half-light radius was calculated as $a_e = \frac{r_e(1-\epsilon)}{1-\epsilon \cos(|PA-MA|)}$, with ϵ being the ellipticity (data from NED), r_e the radius containing half the light of the galaxy (computed from the 2MASS K -band 20 th magnitude arcsec⁻² isophotal radius), PA the slit position axis and MA the major axis.

et al. (2005) found a mild trend between $FUV - NUV$ and Mg_2 in a sample of early-type galaxies in the Virgo cluster. On the other hand, Rich et al. (2005) detected no significant correlation between the $FUV - r$ colour and the Mg_2 index or the velocity dispersion, using a large sample of SDSS early-type galaxies observed with *GALEX*. It is possible that this relation is diluted by lenticular galaxies, as shown in Donas et al. (2007). This correlation has not been previously investigated specifically for BCGs, and even though we do not find a statistically significant correlation between $Mg\,b$ (or Mg_2 – not shown) and UV upturn here, the properties are less scattered compared to our control sample of normal ellipticals.

6 SUMMARY

We compare the stellar population properties derived from optical spectroscopic data with *GALEX* UV colour measurements for 36 nearby BCGs to provide a systematical comparison between the UV upturn in BCGs with that of ordinary massive elliptical galaxies. We also test recent model predictions on the origin of the UV upturn, specifically in central cluster galaxies. To do this, we analyse possible correlations between the $FUV - NUV$ colours and the internal properties of the galaxies (velocity dispersion and luminosity) and those of the host clusters (mass, distance from the BCG to X-ray peak and presence of cooling flows).

We pay particular attention to the model of Peng & Nagai (2009). They pointed out that the helium sedimentation process can greatly increase the helium abundance in BCGs making them conducive to the formation of UV-bright HB stars. It has long been suggested that helium sedimentation occurs in the ICM of galaxy clusters, and under the influence of gravity, the heavier nuclei in the H–He-dominated ICM accumulate at the centres of the clusters. Thus, measuring the UV upturn in BCGs compared to ordinary massive elliptical galaxies should provide a test of this scenario.

Our main conclusions are as follows.

(i) We find significant differences between the UV-upturn distributions between BCGs and normal ellipticals in the same mass range in that the BCGs have higher UV upturns and are less scattered than the normal ellipticals.

(ii) We do not find strong evidence in our data to support the predictions made from the models of Peng & Nagai (2009) that the UV-upturn phenomena should be most pronounced in BCGs hosted by high-mass, dynamically relaxed, cooling flow systems as a result of helium sedimentation.

(iii) We find no clear correlation between the BCG velocity dispersion (mass) and the UV upturn, but we find the UV upturn of the BCG sample to be much less scattered with velocity dispersion than the non-BCGs over the same mass range. We also find no clear correlation between the UV upturn and luminosity, but the BCGs are less scattered than the normal ellipticals.

(iv) We do not find the UV-upturn– Mg correlation reported for some samples of ordinary elliptical galaxies (Burstein et al. 1988; Donas et al. 2007), but we do find that the values are much less scattered than those of the normal elliptical sample that we use as reference. No correlations between the age, metallicity and α -abundance of the BCGs with UV upturn were found.

The UV upturn is the most variable photometric feature associated with old stellar populations, yet it seems that the influence of the cluster environment is limited to enhancing the UV upturn in BCGs compared to non-BCGs and independent of the specific properties of the host cluster (also see Atlee et al. 2009). This absence of correlations with host cluster properties makes it difficult to in-

voke the helium sedimentation scenario as the primary mechanism responsible for the UV upturn.

On both the theoretical and observational grounds, the lifetime UV outputs of these old HB stars are very sensitive to their physical properties (e.g. helium abundance). More remarkably, changes of only a few $0.01 M_{\odot}$ in the mean envelope mass of an extreme HB population can significantly affect the UV spectrum of an elliptical galaxy (O’Connell 1999). If this interpretation is correct, then *FUV* observations become a uniquely delicate probe of the star formation and chemical enrichment histories of elliptical galaxies, but only once we understand the basic astrophysics of these advanced evolutionary phases so that we can explain the diversity in UV observations.

ACKNOWLEDGMENTS

We thank the anonymous referee for constructive comments which contributed to the improvement of this paper. SIL gratefully acknowledges funding from the South African SKA project and thanks Russell Johnston for helpful discussions. PSB is supported by the Ministerio de Ciencia e Innovación (MICINN) of Spain through the Ramon y Cajal programme. This work has been supported by the Programa Nacional de Astronomía y Astrofísica of the Spanish Ministry of Science and Innovation under the grant AYA2007-67752-C03-01.

REFERENCES

- Abramopoulos F., Chanan G. A., Ku W. H.-M., 1981, *ApJ*, 248, 429
 Atlee D. W., Assef R. J., Kochanek C. S., 2009, *ApJ*, 694, 1539
 Baldwin J. A., Phillips M. M., Terlevich R., 1981, *PASP*, 93, 5
 Bautz L. P., Morgan W. W., 1970, *BAAS*, 2, 294
 Bertin E., Arnouts S., 1996, *A&AS*, 117, 393
 Bildfell C., Hoekstra H., Babul A., Mahdavi A., 2008, *MNRAS*, 389, 1637
 Bohringer H. et al., 2000, *ApJS*, 129, 435
 Bohringer H. et al., 2004, *A&A*, 425, 367
 Boselli A. et al., 2005, *ApJ*, 629, 29
 Bruzual G., Charlot S., 2003, *MNRAS*, 344, 1000
 Burke D. J., Collins C. A., Mann R. G., 2000, *ApJ*, 532, 105
 Burstein D., Bertola F., Buson L. M., Faber S. M., Lauer T. R., 1988, *ApJ*, 328, 440
 Cardelli J. A., Clayton G. C., Mathis J. S., 1989, *ApJ*, 345, 245
 Chuzhoy L., Nusser A., 2003, *MNRAS*, 342, 5
 Code A. D. D., Welch G. A., 1979, *ApJS*, 228, 95
 Crawford C. S., Allen S. W., Ebeling H., Edge A. C., Fabian A. C., 1999, *MNRAS*, 306, 857
 Cruddace R. et al., 2002, *ApJS*, 140, 239
 D’Antona F., Caloi V., 2004, *ApJ*, 611, 871
 D’Antona F., Cardini D., Di Mauro M. P., Maceroni C., Mazzitelli I., Montalbán J., 2005, *MNRAS*, 363, 847
 De Lucia G., Blaizot J., 2007, *MNRAS*, 375, 2
 Donahue M. et al., 2010, *ApJ*, 715, 881
 Donas J. et al., 2007, *ApJS*, 173, 597
 Dorman B., O’Connell R. W., Rood R. T., 1995, *ApJ*, 442, 105
 Edwards L. O. V., Hudson M. J., Balogh M. L., Smith R. J., 2007, *MNRAS*, 379, 100
 Ettori S., Fabian A. C., 2006, *MNRAS*, 369, 42
 Gil de Paz A. et al., 2007, *ApJS*, 173, 185
 Gilfanov M. R., Syunyaev R. A., 1984, *Soviet Astron. Lett.*, 10, 137
 Giovannini G., Liuzzo E., Giroletti M., 2008, in Hagiwara Y., Fomalont E., Tsuboi M., Murata Y. eds, *ASP Conf. Ser. Vol. 402, Approaching Micro-Arsecond Resolution with VSOP-2: Astrophysics and Technology*. Astron. Soc. Pac., San Francisco, p. 163
 Han Z., Podsiadlowski P., Lynas-Gray A. E., 2007, *MNRAS*, 380, 1098
 Hicks A. K., Mushotzky R., 2005, *ApJ*, 635, 9
 Hicks A., Mushotzky R. F., Donahue M., 2010, *ApJ*, 719, 1844

- Katayama H., Hayashida K., Takahara F., Fukita Y., 2003, *ApJ*, 585, 687
 Kron R. G., 1980, *ApJS*, 43, 305
 Lamareille F., Mouchine M., Contini T., Lewis I., Maddox S., 2004, *MNRAS*, 350, 396
 Ledlow M. J., Voges W., Owen F. N., Burns J. O., 2003, *AJ*, 126, 2740
 Lee Y.-W. et al., 2005, *ApJ*, 621, L57
 Loubser S. I., Sansom A. E., Sánchez-Blázquez P., Soechting I. K., Bromage G., 2008, *MNRAS*, 391, 1009 (Paper I)
 Loubser S. I., Sánchez-Blázquez P., Sansom A. E., Soechting I. K., 2009, *MNRAS*, 398, 133 (Paper II)
 Martel A. R., Sparks W. B., Allen M. G., Koekemoer A. M., Baum S. A., 2002, *AJ*, 123, 1357
 Martin D. C. et al., 2005, *ApJ*, 619, L1
 Mittaz J. P. D. et al., 2001, *A&A*, 365, 93
 Morrissey P. et al., 2005, *ApJ*, 619, 7
 Norris J. E., 2004, *ApJ*, 612, 25
 O'Connell R., 1999, *ARA&A*, 37, 603
 O'Dea C. P., Baum S. A., Mack J., Koekemoer A. M., Laor A., 2004, *ApJ*, 612, 131
 O'Dea C. P. et al., 2010, *ApJ*, 719, 1619
 Oke J. B., Gunn J. E., 1983, 266, 713
 Patel P., Maddox S., Pearce F. R., Aragón-Salamanca A., Conway E., 2006, *MNRAS*, 370, 851
 Peng F., Nagai D., 2009, *ApJ*, 705, L58
 Perez C. B., Fabian A. C., Edge A. C., Allen S. W., Johnstone R. M., White D. A., 1998, *MNRAS*, 298, 416
 Piotto G. et al., 2005, *ApJ*, 621, 777
 Pipino A., Kaviraj S., Bildfell C., Hoekstra H., Babul A., Silk J., 2009, *MNRAS*, 395, 462
 Qin B., Wu X.-P., 2000, *ApJ*, 529, 1
 Quillen A. C. et al., 2008, *ApJS*, 179, 39
 Rafferty D. A., McNamara B. R., Nulsen P. E. J., Wise M. W., 2006, *ApJ*, 652, 216
 Rafferty D. A., McNamara B. R., Nulsen P. E. J., 2008, *ApJ*, 687, 899
 Rampazzo R. et al., 2007, *MNRAS*, 381, 245
 Ree C. H. et al., 2007, *ApJS*, 173, 607
 Rich R. et al., 2005, *ApJ*, 619, L107
 Rood H. J., Sastry G. N., 1971, *PASP*, 83, 313
 Sánchez-Blázquez P., Gorgas J., Cardiel N., González J. J., 2006, *A&A*, 457, 787 (SB06)
 Sandage A., Visvanathan N., 1978, *ApJ*, 223, 707
 Sarzi M. et al., 2006, *MNRAS*, 366, 1151
 Schlegel D. J., Finkbeiner D. P., Davis M., 1998, *ApJ*, 500, 525
 Stasińska G., Cid Fernandes R., Mateus A., Sodré L., Asari N. V., 2006, *MNRAS*, 371, 972
 Struble M. F., Rood H. J., 1991, *ApJS*, 77, 363
 Struble M. F., Rood H. J., 1999, *ApJS*, 125, 35
 Thomas D., Maraston C., Bender R., 2003, *MNRAS*, 343, 279
 Thomas D., Maraston C., Korn A. J., 2004, *MNRAS*, 351, 19
 Von der Linden A., Best P. N., Kauffmann G., White S. D. M., 2007, *MNRAS*, 379, 867
 Wang J., Overzier R., Kauffmann G., Von der Linden A., Kong X., 2010, *MNRAS*, 401, 433
 White D. A., Jones C., Forman W., 1997, *MNRAS*, 292, 419
 Wyder T. K. et al., 2007, *ApJS*, 173, 293
 Yi S. K., 2008, in Heber U., Jeffery S., Napiwotzki R. eds, *ASP Conf. Ser. Vol. 392, Hot Subdwarf Stars and Related Objects*. Astron. Soc. Pac., San Francisco, p. 3
 Yi S. K., Yoon S.-J., 2004, *Ap&SS*, 291, 205
 Yi S., Demarque P., Oemler A., 1997, *ApJ*, 486, 201

APPENDIX A: BCG PROPERTIES

Photometric measurements of the BCGs, and X-ray properties and velocity dispersions of the host clusters for all 36 BCGs are listed in Table A1. The velocity dispersions and photometric measurements of the SB06 ellipticals used here are listed in Table A2.

Table A1. Velocity dispersions and photometric measurements of the BCGs, and X-ray properties and velocity dispersions of the host clusters. The BCG σ and σ_{cluster} values are in km s^{-1} and the projected distance between the galaxy and the cluster X-ray peak (R_{off}) is in Mpc. The \star marks at R_{off} indicate that the galaxy is not in the centre of the cluster but closer to a local maximum X-ray density, different from the X-ray coordinates given in the literature. The references are as follows: w = White et al. (1997); e = Edwards et al. (2007); g = Giovannini et al. (2008); r = Rafferty et al. (2006); cc = Calculated from Bohringer et al. (2000); cl = Calculated from Ledlow et al. (2003); cb = Calculated from Bohringer et al. (2004); cr = Calculated from Cruddace et al. (2002); st = Struble & Rood (1999); s = Struble & Rood (1991); p = Patel et al. (2006) and pe = Perez et al. (1998). All the values for T_X are from White et al. (1997).

Galaxy	Cluster	BCG σ (km s^{-1})	<i>NUV</i> (mag)	<i>FUV</i> (mag)	<i>K</i> band (mag)	T_X (keV)	Cooling flow ref	σ_{cluster} (km s^{-1})	ref	R_{off} (Mpc)	ref	
ESO 202-043	A S0479	256	19.28 ± 0.15	20.35 ± 0.30	-25.98	-	-	-	-	-	-	
ESO 303-005	RBS521	276	19.64 ± 0.12	20.67 ± 0.22	-25.39	-	-	-	-	0.010	cb	
ESO 346-003	A S1065	226	18.74 ± 0.05	19.53 ± 0.12	-25.60	-	-	-	-	0.032	cr	
ESO 444-046	A3558	292	18.44 ± 0.03	19.28 ± 0.08	-27.00	3.8	×	e	w	986	e	
ESO 488-027	A0548	248	18.71 ± 0.03	19.96 ± 0.11	-25.94	2.4	✓	w	w	853	★	
ESO 541-013	A0133	295	19.41 ± 0.15	19.77 ± 0.24	-26.41	3.8	✓	w, r	w	767	e	
ESO 552-020	CID 28	229	19.13 ± 0.14	19.33 ± 0.24	-26.39	-	-	-	-	-	0.013	cb
IC 1101	A2029	378	18.89 ± 0.04	19.56 ± 0.07	-27.52	7.8	✓	w, r	w	786	p	
IC 1633	A2877	400	17.59 ± 0.02	18.19 ± 0.01	-26.61	3.5	×	w	w	738	cb	
Leda 094683	A1809	332	20.55 ± 0.08	21.35 ± 0.14	-26.68	3.7	✓	w	w	249	p	
NGC 0533	A0189B	299	17.43 ± 0.04	18.17 ± 0.07	-26.04	-	-	-	-	-	0.004	cb
NGC 0541	A0194	246	18.03 ± 0.02	19.26 ± 0.05	-25.13	1.9	×	w	w	480	0.037	cb
NGC 1399	RBS454	371	15.23 ± 0.02	15.56 ± 0.02	-24.86	-	✓	w	w	240	<0.001	cb
NGC 1713	CID 27	251	19.18 ± 0.17	20.33 ± 0.48	-24.88	-	-	-	-	-	-	-
NGC 2832	A0779	364	17.74 ± 0.01	18.53 ± 0.03	-26.30	1.5	✓	w	w	503	0.038	cl
NGC 3311	A1060	196	17.60 ± 0.07	18.02 ± 0.13	-25.51	3.3	✓	w	w	608	0.015	pe
NGC 3842	A1367	287	17.42 ± 0.01	18.27 ± 0.02	-25.70	3.5	✓	w	w	822	0.252	e
NGC 4839	A1656	278	17.42 ± 0.02	18.34 ± 0.04	-25.96	-	-	-	-	-	★	-
NGC 4874	A1656	267	18.10 ± 0.08	18.71 ± 0.25	-26.24	8.0	×	w, e, g	w	1010	0.038	cb
NGC 4889	A1656	380	17.52 ± 0.05	18.08 ± 0.12	-26.49	8.0	×	w, e, g	w	1010	0.169	e
NGC 6034	A2151	325	19.88 ± 0.12	20.90 ± 0.36	-25.39	3.5	×	w, g	w	827	★	-
NGC 6086	A2162	318	19.43 ± 0.15	19.83 ± 0.27	-25.72	-	×	g	s	323	0.053	cl

Table A1 – continued

Galaxy	Cluster	BCG σ (km s ⁻¹)	NUV (mag)	FUV (mag)	K band (mag)	T_X (keV)	Cooling flow ref	σ_{cluster} (km s ⁻¹)	ref	R_{off} (Mpc)	ref
NGC 6160	A2197	266	18.56 ± 0.06	19.51 ± 0.28	-25.92	1.6	✓	564	w, g	0.017	cc
NGC 6166	A2199	310	17.44 ± 0.02	18.18 ± 0.04	-26.45	4.7	✓	794	w, e, g, r	0.007	e
NGC 6173	A2197	304	18.22 ± 0.02	19.54 ± 0.02	-26.19	-	-	-	-	★	-
NGC 6269	AWM5	343	19.44 ± 0.16	20.14 ± 0.29	-26.51	-	-	-	-	0.002	cc
NGC 7012	A S0921	240	18.52 ± 0.08	19.17 ± 0.23	-26.01	-	-	-	-	-	-
NGC 7597	A2572	264	19.66 ± 0.12	20.06 ± 0.31	-25.84	-	-	676	st	0.048	cc
NGC 7647	A2589	271	18.66 ± 0.03	19.38 ± 0.08	-25.99	3.7	×	500	w	0.073	e
NGC 7649	A2593	250	19.30 ± 0.12	19.66 ± 0.16	-26.24	3.1	×	690	w	0.020	cl
NGC 7768	A2666	272	18.49 ± 0.06	19.75 ± 0.22	-26.04	1.6	×	476	w, g	0.006	cl
PGC 026269	A0780	222	17.96 ± 0.01	18.34 ± 0.03	-	-	✓	641	e,r	0.015	e
PGC 030223	A0978	337	20.37 ± 0.28	21.25 ± 0.50	-26.22	-	-	498	st	0.027	cb
PGC 072804	A2670	311	19.87 ± 0.02	20.51 ± 0.03	-26.92	3.9	✓	1038	w	0.035	cb
UGC 00579	A0119	246	18.99 ± 0.03	19.90 ± 0.05	-26.46	5.1	×	863	w, e	0.054	e
UGC 10143	A2147	262	19.15 ± 0.08	20.23 ± 0.26	-	4.4	×	1148	w, e, g	0.082	e

Table A2. The velocity dispersions and photometric measurements of the control sample of ellipticals.

Galaxy	σ (km s ⁻¹)	NUV (mag)	FUV (mag)	K band (mag)
NGC 2329	229	18.59 ± 0.06	19.48 ± 0.12	-25.16
NGC 3115	284	14.67 ± 0.01	16.11 ± 0.01	-24.09
NGC 3379	228	15.10 ± 0.01	16.49 ± 0.01	-23.77
NGC 4261	303	15.81 ± 0.01	16.79 ± 0.01	-25.14
NGC 4278	277	15.47 ± 0.01	16.35 ± 0.01	-23.58
NGC 4365	258	15.06 ± 0.01	16.19 ± 0.01	-24.79
NGC 4472	310	14.48 ± 0.01	15.44 ± 0.03	-25.47
NGC 4594	259	13.82 ± 0.01	14.96 ± 0.01	-25.17
NGC 4621	232	15.45 ± 0.01	16.66 ± 0.01	-24.27
NGC 5796	274	18.01 ± 0.08	18.72 ± 0.14	-24.68
NGC 5812	217	17.60 ± 0.04	18.80 ± 0.12	-24.17
NGC 5813	257	16.33 ± 0.02	17.39 ± 0.03	-24.77
NGC 5854	254	17.03 ± 0.01	19.49 ± 0.05	-22.94
NGC 5846	248	16.07 ± 0.01	16.97 ± 0.02	-25.10
NGC 6127	251	18.10 ± 0.03	18.72 ± 0.12	-24.39
NGC 1453	337	17.44 ± 0.01	18.38 ± 0.03	-25.36
NGC 2300	303	17.00 ± 0.02	17.93 ± 0.03	-25.01
NGC 2693	322	17.36 ± 0.01	18.23 ± 0.02	-25.11
NGC 0315	304	17.31 ± 0.01	18.41 ± 0.03	-25.83
NGC 3608	203	16.24 ± 0.01	17.73 ± 0.01	-23.70
NGC 3665	222	16.33 ± 0.02	17.77 ± 0.08	-24.80
NGC 4374	301	14.75 ± 0.01	16.19 ± 0.01	-24.86
NGC 4552	262	15.30 ± 0.01	14.95 ± 0.01	-24.14
NGC 4649	368	14.34 ± 0.01	15.15 ± 0.01	-25.77
NGC 0507	266	16.84 ± 0.01	18.31 ± 0.03	-25.67
NGC 0584	224	16.20 ± 0.01	18.08 ± 0.03	-24.06
NGC 0821	212	16.93 ± 0.01	18.76 ± 0.06	-23.97
NGC 7052	201	18.89 ± 0.09	18.81 ± 0.25	-25.41
CGC G-159-43	231	19.92 ± 0.14	20.70 ± 0.22	-23.92
IC 3959	226	19.84 ± 0.03	20.51 ± 0.12	-23.69
IC 3973	256	19.88 ± 0.12	20.76 ± 0.37	-22.82
IC 4051	299	19.41 ± 0.04	20.85 ± 0.13	-24.61
NGC 4842A	232	19.78 ± 0.03	20.52 ± 0.09	-23.96
NGC 4864	221	19.61 ± 0.13	20.57 ± 0.27	-23.98
NGC 4865	308	19.26 ± 0.09	20.35 ± 0.20	-23.50
NGC 4867	247	19.63 ± 0.11	20.66 ± 0.24	-23.57
NGC 4908	201	18.55 ± 0.03	19.51 ± 0.06	-24.44

 This paper has been typeset from a \LaTeX file prepared by the author.